Renewable resources derived aliphatic hyperbranched polyurethane

Highlight

This chapter describes the synthesis, characterization, property evaluation and potential application of renewable resource-derived purely aliphatic hyperbranched polyurethane (HPU). This chapter elaborates on the synthesis of a castor oil-modified polyol as a multi-functional moiety, and its subsequent utilization in the pre-polymerization technique-driven synthesis of purely aliphatic HPU by $A_x + B_y$ ($x, y \geq 2$) approach without using any catalyst. The synthesized polymer is well characterized by various spectroscopic and analytical techniques. The synthesized HPU illustrates a plethora of remarkable features like mechanical stability, chemical resistance, biodegradability, UV-resistance and shape memory attribute. The chapter delves into the elucidation of the overall results and substantiates the potential of the synthesized HPU as a multi-faceted material.

Portions of this chapter are published in:

Bayan, R. and Karak, N. Renewable resource modified polyol derived aliphatic hyperbranched polyurethane as a biodegradable and UV-resistant smart material. *Polymer International*, 66(6):839-850, 2017.

2.1. Introduction

Chapter 1 clearly communicates the necessity and usefulness of renewable resource based polymers in tackling the global polymer woes. Use of renewable resources as an alternative to petrochemical feedstock in polymer production paves the way for development of eco-friendly and resourceful polymeric materials [1, 2]. In this regard, vegetable oils represent a good viable option as renewable feedstock for polymer production. They offer numerous advantages in terms of easy availability, economic viability, versatility in structure and property, environmental safety and most importantly, biodegradability [3-7]. Such ideal features make them suitable as renewable resource based precursor for synthesis of polymers.

As discussed in **Chapter 1**, PU presents an ideal polymeric template for the development of highly resourceful polymeric materials. The judicious customization of the structure and composition of their basic building blocks offer ample scope for tuning the attributes of PU [6]. This includes development of HPU having unique three-dimensional, less-entangled, globular, highly functionalized architectural features with desirable properties like high solubility, low solution and melt viscosity, good compatibility with others, etc [8-10]. Design of such uniquely structured HPU considerably supplements their material aspects [6, 10].

In this context, utilization of vegetable oils as renewable resource in synthesis of HPU provides a good opportunity to develop eco-friendly polymeric materials. It is also learnt that further modification or functionalization of vegetable oil with suitable monomeric units compensate for its moderate reactivity and forms an interesting tactic to obtain HPU with additional chemical functionalities in addition to urethane [11-13]. In many occasion, incorporation of additional linkages and chemical functionalities often seems desirable to enhance various material properties [14, 15]. Of late, aliphatic PUs is less explored in terms of academic interest and applicability. Aliphatic PU with its structure comprising of saturated long chain moieties show light stability and excellent optical clarity [16, 17]. Besides, the presence of long aliphatic chains may also imbue flexibility and hydrophobic character in the polymer. In such circumstance, use of vegetable oil modified or functionalized precursor with its inherent aliphatic nature may direct an interesting strategy for development of aliphatic HPUs. Among different vegetable oils, castor (*Ricinus communis*) oil is a comparatively inexpensive and easily available vegetable oil, comprising primarily of triricinolein, a triglyceride of ricinoleic acid (92-95%) with secondary hydroxyl groups in their long fatty acid chains [3, 4, 6]. Hence, the use of castor oil as polyol source can pay rich dividends in production of economic and performance-oriented HPU.

In this perspective, a simple strategy of using a castor oil-modified polyol as a multi-functional branching precursor, along with other conventional reactants for the synthesis of purely aliphatic HPU was reported. Various sophisticated spectroscopic and analytical techniques were employed for the characterization of the synthesized HPU. Various properties of HPU including mechanical and thermal were evaluated. Additionally, chemical resistance, biodegradability, UV-aging and shape memory behavior of HPU were investigated and discussed in the chapter to highlight its potential as an eco-friendly multi-faceted material.

2.2. Experimental

2.2.1. Materials

Poly(*ε*-caprolactone)diol (PCL) was employed as the macrogylcol in the synthesis of linear PU and HPU. PCL is a polyester based dihydroxy compound having a waxy solid appearance with number average molecular weight of 2000 g mol^{-1}, hydroxyl number of 54 mg KOH g^{-1} and melting point of 50 °C. It was procured from Sigma Aldrich, USA and used as received after vaccum drying at 45 °C for 24 h.

Isophorone diisocyanate (IPDI) was utilized as the diisocyanate in the synthesis of linear PU and HPU. It is an aliphatic diisocyanate compound having a colorless and odorless liquid appearance, with molecular weight of 222.28 g mol^{-1}, density of 1.049 g cm^{-3} and boiling point of 158 °C. IPDI was purchased from Sigma Aldrich, Germany, as a mixture of *cis*- and *trans*-isomers in the ratio of 3:1 and used as received.

1,4-Butanediol (BD) was used as a chain extender in the synthesis of linear PU. It is a dihydroxy compound with colorless appearance, having molecular weight of 90.12 g mol^{-1}, density of 1.02 g cm^{-3} and boiling point of 230 °C. BD was obtained from Merck, India and vacuum dried at 45 °C for 24 h prior to use.

Helianthus annuus seed oil or sunflower oil (SO) was used as a renewable precursor in the preparation of the chain extender, for the synthesis of HPU. It has a density of 0.92 g mL^{-1}, mainly consists of polyunsaturated acid (mostly linoleic acid), monounsaturated fatty acid (oleic acid) and saturated fatty acids (stearic and palmitic acids). SO was purchased from Sigma Aldrich, Germany and used after vacuum dried at 45 °C for 24 h before use. SO served as the triglyceride that was converted to its monoglyceride (MGE) by transesterification reaction as per previously reported method [18].

Ricinus communis seed oil or castor oil (CO) was employed as a renewable precursor in preparation of the branch generating moiety, for the synthesis of HPU. It has density of 0.961 g mL^{-1}, boiling point of 313 °C and is composed of mainly

monounsaturated fatty acid (ricinoleic and oleic acids), polyunsaturated acid (mostly linoleic acid) and saturated fatty acids (stearic and palmitic acids). CO was procured from Sigma Aldrich, Germany and dried in vacuum at 60 °C for 24 h before use.

Diethanolamine (DEA) was used as a precursor in the preparation of the branch generating moiety, for the synthesis of HPU. It is a dihydroxyamine compound with molecular weight of 105.14 g mol^{-1}, density of 1.09 g cm^{-3}, melting point of 28 °C and boiling point of 270 °C. It was obtained from Merck, India and used after vacuum drying at 60 °C for 24 h.

Glycerol was used as a precursor in the preparation of the chain extender, for the synthesis of HPU. It has a density of 1.26 g mL^{-1} with minimum assay 99%, molecular weight of 90.09 g mol^{-1}. Glycerol was procured from Merck, India and dried in vacuum drying at 60 °C for 24 h prior to use. It served as a triol (alcoholyzing reagent) for converting the triglyceride of SO into the chain extender MGE.

Calcium oxide (CaO) was used as a catalyst for transesterification reaction of triglyceride of SO with glycerol to prepare the chain extender MGE. CaO with minimum assay of 99% was purchased from Merck, India and used directly.

Xylene was employed as the solvent for the synthesis of HPU. It is a colorless liquid with molecular weight of 106.16 g mol^{-1}, density of 0.864 g cm^{-3} and boiling point of 138.5 °C. It was bought from Merck, India, vacuum distilled and stored in 4A type molecular sieves prior to use.

Molecular sieve of 4A type was used to entrap trace quantities of moisture in solvents. It is a bead-like solid with equilibrium capacity for water around 20% at 30 °C and 75% relative air humidity. It was procured from Merck, India and pre-heated at 60 °C for 5 h prior to use.

Sodium chloride (NaCl) 10% (w/v) aqueous solution was used to assess the chemical resistance of HPU films under saline conditions. NaCl crystals having purity 99.5%, molecular weight of 58.44 g mol^{-1} and density of 2.16 g cm^{-3} were procured from Merck, India and used as received.

Sodium hydroxide (NaOH) 10% (w/v) aqueous solution was used to assess the chemical resistance of HPU films under alkali conditions. NaOH pellets having purity 97%, molecular weight of 39.99 g mol^{-1} and melting point of 319 °C were procured from Merck, India and used as received.

Hydrochloric acid (HCl) 5% (v/v) aqueous solution was used to assess the chemical resistance of HPU films under acidic conditions. HCl of 37% strength (~11.6 M), molecular weight of 36.5 g mol^{-1} and density of 1.19 g cm^{-3} (at 20 °C) was procured from Merck, India and diluted to 5% (v/v) solution.

Bacterial strain of *Pseudomonas aeruginosa* (*P. aeruginosa*) (MTCC 7814) was used in the biodegradation study. It was procured from Microbial Type Culture Collection and Gene Bank, Chandigarh, India. The bacterial culture was supplied by the Department of Molecular Biology and Biotechnology, Tezpur University, Assam, India.

2.2.2. Methods

2.2.2.1. Synthesis of castor oil modified polyol (COMP)

Vacuum dried CO and DEA in the molar ratio of 1:4 were taken in a three-necked round bottomed flask immersed in a pre-heated oil bath, equipped with an overhead mechanical stirrer, a nitrogen gas inlet and a thermometer. The reactants were subjected to heating at 120 °C for 4-5 h with constant mechanical agitation and nitrogen flow. After, completion of the reaction, the product was allowed to cool, collected in a reagent glass bottle and stored inside a vacuum desiccator. COMP was obtained as a yellow oily liquid with quantitative yield. The structural characterization of COMP was performed by FTIR and NMR spectroscopy.

2.2.2.2. Synthesis of HPU

Purely aliphatic HPU was synthesized by pre-polymerization technique using reaction set-up of a three-necked round-bottomed flask, outfitted with a mechanical stirrer, a nitrogen gas inlet, a thermometer and a Teflon septum. In the first step, definite amounts of PCL were taken in the reaction flask containing small amount of xylene as solvent under constant mechanical stirring. After dissolving PCL, a specific amount of IPDI was then slowly injected into the reaction flask at room temperature under constant mechanical agitation. The reactants were gradually heated to 130±5 °C and then allowed to react for 3 h. The highly viscous mass obtained at the end of the first step was considered as the pre-polymer. For different compositions, NCO/OH ratio of the reaction varied from 1.3 to 1.5 in the first step to give an isocyanate-terminated pre-polymer, which was confirmed by the presence of free isocyanate (–NCO) band at 2270 cm^{-1} in FT-IR spectrum [12].

The pre-polymer was then cooled to room temperature and definite amounts of the multi-functional moiety COMP, chain extender MGE and IPDI were added under constant mechanical agitation by maintaining an NCO/OH ratio of 1.0. The reactants were gradually re-heated to 130±5 °C and allowed to react for 3 h, till the completion of the reaction as indicated by the formation of a highly viscous mass and confirmed by the absence of free isocyanate (–NCO) band at 2270 cm^{-1} in FT-IR spectrum [12]. The synthesized polymer was cooled to room temperature, collected in a glass container and stored in a desiccator. Following the same procedure, HPUs were synthesized with three different compositions of

multi-functional moiety COMP and coded as HPU1, HPU2 and HPU3. Further, renewable resource based linear PU (coded as BLPU) and synthetic linear PU (coded as LPU) was also synthesized using the same technique for comparison purpose. The compositions of the reactants in mmol and other parameters in percentage for the synthesized PUs are provided in **Table 2.1**.

Table 2.1. Compositions of the reactants in mmol and other parameters in percentage for PUs

Composition	HPU1	HPU2	HPU3	BLPU	LPU
PCL	4.5	4.5	4.5	4.5	4.5
MGE	5.0	5.0	5.0	5.0	-
BD	-	-	-	1.3	6
COMP	0.6	1.0	1.3	-	-
IPDI	10	10	10	10	10
Hard Segment %	36	37	38	36	30
Soft Segment %	64	63	62	64	70
Branching Unit %	1.5	2.3	3.1	-	-
Renewable source %	16	17	18	15	-

2.2.2.3. Sample preparation for performance study

All PU compositions were processed into thin films by solution casting onto glass slides (7.5 cm × 2.5 cm × 0.139 cm) and mild steel plates (15 cm × 10 cm × 0.144 cm), followed by complete drying for 24 h under ambient conditions. The dried PU films were peeled off from the glass slides by immersing in hot water, dried under vacuum for 24 h and used for various testing. For mechanical testing, the dried PU films were cut into small strips of dimensions 5 cm × 1.2 cm and thickness in the range of 0.4-0.6 mm. In case of impact resistance testing, PU cast mild steel plates were directly used.

A small sample of HPU composition was purified by precipitation in deionized water and dried under vacuum oven at 50 °C for NMR spectral analysis only. All other analyses and testing were performed using bulk PU samples without any further purification.

2.2.2.4. Biodegradation study

Biodegradation study of the PUs was conducted by using *P. aerugonisa* as the bacterial strain. In brief, a nutrient medium of mineral salts containing 2.0 g of Na_2HPO_4, 4.75 g of

KH_2PO_4, 2.0 g of $(NH_4)_2SO_4$, 1.2 g of $MgSO_4 \cdot 7H_2O$, 0.07 g of $ZnSO_4 \cdot 7H_2O$, 0.01 g of $H_3BO_3 \cdot 5H_2O$, 0.005 g of $CaCl_2 \cdot 2H_2O$, 0.1 g of $MnSO_4 \cdot 5H_2O$, 0.1 g of $CuSO_4 \cdot 7H_2O$, 0.001 g of $FeSO_4 \cdot 7H_2O$, and 0.01 g of MoO_3 was prepared in 1 L of de-ionized water. The medium was sterilized in an autoclave at 120 °C and 15 lb pressure for 30 min. Bacterial strain of *P. aerugonisa* was cultured in the nutrient medium inside an incubator shaker at 37 °C for 48 h. The PU film samples were initially sterilized by exposure to UV light (254 nm) for 15 min. The sterilized PU films (in duplicates) were then immersed in culture tubes containing 15 mL of nutrient medium, inoculated with 100 µL (10^8 microbes mL^{-1}, as calculated by McFarland turbidity standards) of the cultured bacterial medium and incubated at 37 °C for a period of 7 weeks. A medium without PU film was set as the negative control. Bacterial growth was indicated by the increase in the turbidity of the medium with time. The optical density (OD) of the bacterial medium was examined by monitoring the absorbance at 600 nm with the help of a UV-Vis spectrophotometer with respect to the control [19]. The extent of biodegradation was gauged by measuring the weight loss (%) of the degraded PU films, after 7 weeks of exposure to the bacterial strain, based on the following equation.

$$\text{Weight loss (\%)}, W = \frac{W_0 - W_t}{W_t} \times 100 \qquad \textbf{(Eq. 2.1)}$$

where W_0 and W_t are the weights of the sample before and after degradation, respectively, at the time of interest, t.

Additionally, biodegradation of the PU films was studied by scanning electron microscope (SEM) images of the degraded films after 7 weeks of bacterial degradation.

2.2.2.5. UV-resistance study

UV-resistance study of the PUs was performed by exposing the PU films to UV radiation and evaluating any changes in their mechanical properties. PU films were exposed to UV radiation of wavelength 254 nm inside a UV chamber under ambient conditions for a total duration of 2 weeks. Subsequently, the films were subjected to testing of mechanical properties, i.e. tensile strength, elongation at break and toughness, in order to evaluate the retention (%) of properties, determined by the following equation.

$$\text{Retention, } R\,(\%) = \left[100 - \left|\frac{P_0 - P_1}{P_1}\right|\right] \times 100 \qquad \textbf{(Eq. 2.2)}$$

where, P_0 and P_1 signify values of the mechanical property before and after UV-aging.

2.2.2.6. Shape memory study

Shape memory behavior of the PU films was studied by performing the bending test. The shape fixity of the samples was accomplished by heating the films at 65 °C for 5 min and

folding them in form of a temporary ring shape, followed by instant quenching in an ice water-salt bath at −5 °C for 15 min. After attaining the temporary fixed shape, the shape fixity of the sample was calculated by drying the films under vacuum and keeping them at room temperature for 30 min. Thereafter, the shape recovery of the temporary deformed films was achieved by using different stimuli *viz.* thermal energy, microwave and sunlight and the time required for the films to attain original shape duly noted with a stop-watch. For thermal energy triggered shape recovery of the films, the temporary fixed samples were immersed in a vessel containing warm water at 50 °C. After shape recovery, the samples were taken out and dried under ambient conditions. Similarly, microwave activated shape recovery was accomplished by placing the deformed sample inside a domestic microwave operating at a power of 450 W. Following shape recovery, the sample was cooled and dried under room temperature. The sunlight induced shape recovery was attained with the samples being exposed directly to sunlight in sunny days of June, 2016, with light intensity of 10^5 lux. Subsequently, the shape recovered films were removed from sunlight and kept under ambient conditions. The shape fixity of the deformed films and their shape recovery were evaluated by using Eq. 1.4 & 1.5, as described previously in Chapter 1.

2.2.3. Characterization

Fourier transform infrared (FT-IR) spectra of COMP and PUs were obtained by an IR spectrophotometer (Model: Impact 410, Nicolet, USA), using KBr as the standard. ^{1}H and ^{13}C Nuclear Magnetic Resonance (NMR) spectra of COMP and HPU were recorded by a 400 MHz NMR instrument (Model: ECS-400, JEOL, Japan) with chloroform-d_1 ($CDCl_3$) as the solvent and tetramethylsilane (TMS) as an internal standard. Molecular weight and polydispersity index of HPU were determined by Gel Permeation Chromatography (GPC) instrument (Model: UV/V Visible detection-2489, Refractive Index detector-2414, HPLC pump-515, Waters Corp., UK). Specific gravity of HPU was evaluated by a pycnometer at room temperature (~28 °C) using the conventional liquid displacement method (Archimedes' principle). X-ray diffraction (XRD) patterns of the PUs were obtained using a small-angle XRD machine (Model: D8 FOCUS, Bruker AXS, Germany) operating with Cu-Kα as the irradiation source. Thermal degradation profiles of PUs were studied by Thermogravimetric analyzer (TGA) instrument (Model: TGA 4000, Perkin Elmer, USA) in the temperature range of 32°C to 720 °C, at a scanning rate of 10 °C min^{-1} by maintaining an inert atmosphere of nitrogen at a gas flow rate of 30 mL min^{-1}. Glass transition and melting transition temperatures of PUs were measured by Differential Scanning Calorimetry (DSC) instrument (Model: DSC 6000, Perkin Elmer, USA) in the temperature

range -70 °C to 100 °C transcending a cycle of heating-cooling-heating under an atmosphere of nitrogen at a scanning rate of 4 °C min^{-1}. A Universal Testing Machine (UTM) (Model: WDW-10, Jinan, China) equipped with a 10 kN load cell, operating at a crosshead speed of 0.05 m min^{-1} was employed to measure the tensile strength and elongation at break of the PU films. Scratch hardness of PU films was assesses by a scratch hardness tester (Model: 705, Sheen Instrument Ltd., UK). Impact resistance of PU films was calculated by a falling weight impact tester (S. C. Dey & Co., India) with a falling weight of 0.85 kg and maximum height of 1 m. Chemical resistance test was performed in different chemical medium, viz. saline, acidic, alkaline, alcoholic and aqueous, as per the ASTM D 543-67 standard procedure for a period of 50 days. Absorbance of the PU films inoculated bacterial culture medium was recorded using an UV-visible spectrophotometer (Model: Evolution-300, ThermoFisher, USA). Surface morphology of the pristine and biodegraded HPUs were analyzed by a Scanning Electron Microscope (SEM) (Model: JSM 6390LV, JEOL, Japan) after platinum coating on the surfaces. The shape memory behavior of HPU films was studied by using a domestic microwave oven (LG, India) operating at a maximum power output of 900 W.

2.3. Results and discussion

2.3.1. Synthesis of COMP

CO, which primarily comprises of triricinolein, a triglyceride of ricinoleic acid was modified to a comparatively more reactive polyol by a single pot, one-step reaction with DEA, as illustrated in **Scheme 2.1**. In this reaction, CO undergoes transamidation reaction with DEA at a high temperature of 120 °C to yield diethanol fatty amide of CO (**1**) as the primary product with some residual amounts of glycerol (**2**) and unreacted diethanolamine (**3**), collectively regarded as COMP.

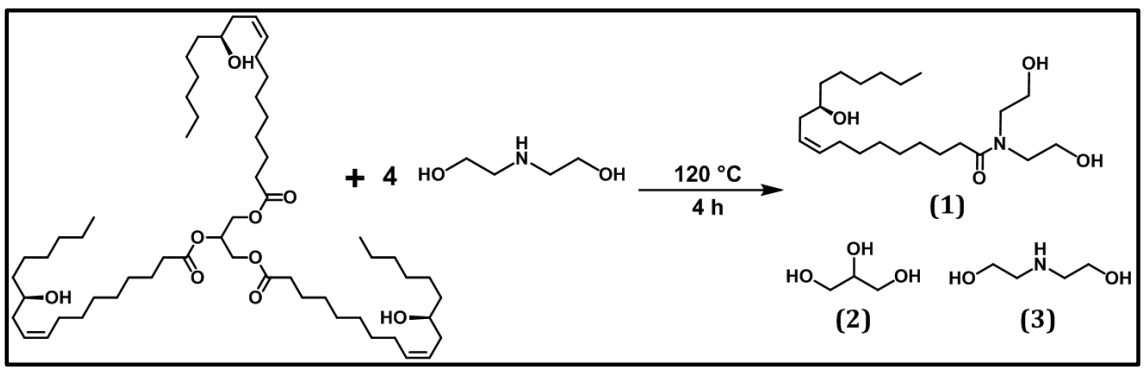

Scheme 2.1. Synthesis of COMP.

COMP was found to be soluble in most of the common polar organic solvents like methanol, ethanol, acetone, xylene, ethyl acetate, THF, DMF, DMAc, DMSO, etc. due to the presence of diverse functional moieties like hydroxyl groups and amide carbonyl groups. Moreover, its solubility in hydrocarbon solvents like xylene and toluene validates the presence of long fatty acid chain in the structure.

2.3.2. Characterization of COMP

2.3.2.1. FT-IR analysis

A comparative study of FT-IR spectra of COMP and CO, as depicted in **Figure 2.1,** reveals prominent changes in their vibrational frequencies and thereby supporting the formation of COMP**.** Most notably, the disappearance of the ester C=O stretching at 1732 cm^{-1} of CO and the emergence of the carbonyl amide at 1620 cm^{-1} affirm the formation of **1 [**20]. The broadening of the O-H peak at 3408 cm^{-1} due to the overlapping of O-H and N-H stretching frequencies asserts the presence of **1,** along with **2** and **3** (Scheme 2.1). Furthermore, the appearance of the C-N stretching frequency of **1** and **3** at 1053 cm^{-1} and N-H (out of plane) bending frequency of **3** at 731 cm^{-1}, gives us further evidence of collective structure of COMP [20, 21].

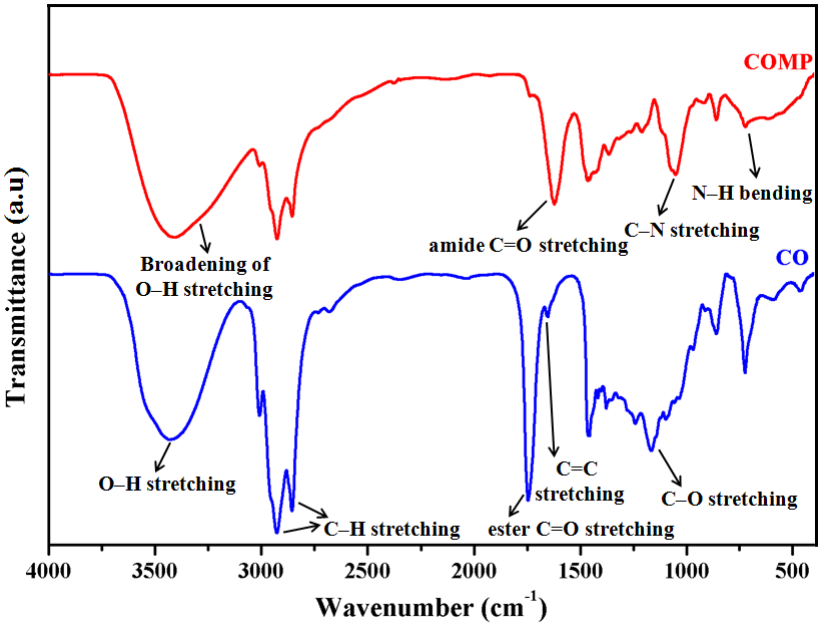

Figure 2.1. FT-IR spectra of CO and COMP.

2.3.2.2. NMR analysis

NMR study of COMP divulges further details of the proposed composition of COMP as a highly functional complex aggregate structural featuring **1, 2** and **3** (Scheme 2.1). ^{1}H NMR spectrum depicted in **Figure 2.2** illustrates the types of protons present in the structure of

COMP. The singlet peak at 0.88 ppm belongs to the terminal methyl (-CH_3) protons of the fatty amide chain of **1,** as well the broad singlet peak near 1.30 ppm is due to the internal methylene (-CH_2) protons [12, 32]. The signal around 1.60 ppm can be ascribed to the beta methylene (β –CH_2) protons to the C=O of the fatty amide chain. The peaks near 2.03 ppm and 2.20 ppm might be assigned to the allylic methylene (-C=C-CH_2) protons of **1** [20]. Further, the singlet peak near 2.38 ppm can be credited to the alpha methylene (α – CH_2) protons to the C=O of **1** [20]**.** The signal near 2.80 ppm belong to N-substituted methylene (-CH_2) protons of **3**. The multitude of signals appearing at 3.48-3.53 ppm and 3.74-3.79 ppm can be attributed to N-substituted methylene (-CH_2) protons of **1** and **3** and O-substituted methylene (-CH_2) protons of **1**, **2** and **3** respectively. The singlet appearing at 3.60 ppm can be connected to methine proton (-CH) attached to the -OH group of **1**. The vinylic (=C-H) protons of **1** emerge as multiplets near 5.55-5.49 ppm, while the free hydroxyl (-OH) protons of **1**, **2** and **3** appear as multiplets around 5.42-5.36 ppm [12, 20-23].

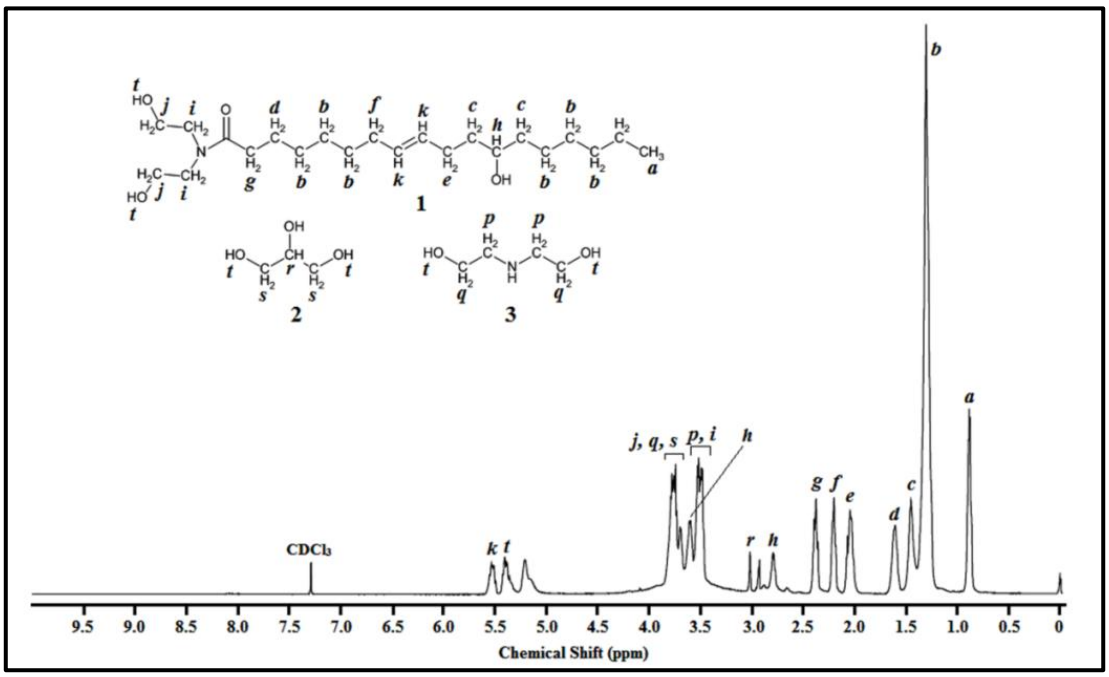

Figure 2.2. ^{1}H NMR spectrum of COMP.

^{13}C NMR spectrum in **Figure 2.3** shows the relevant chemical shifts pertaining to the type of carbon nuclei in the structure of COMP. Chemical shifts (δ_C) at 14.16 ppm and 22.69-36.83 ppm correspond to carbons of the methyl (-CH_3) group and methylene (-CH_2) groups of the fatty acid chain of **1**, respectively [12, 20]. The signals at 50.49 ppm and 50.97 ppm belong to the N-substituted methylene carbons of **1** and **3.** The peaks appearing at 52.28 ppm, 60.64 ppm, 61.12 ppm and 63.06 ppm are assigned to mono-substituted alcoholic

carbons of **3**, **1** and **2** respectively [20-23]. The di-substituted alcoholic carbons of **1** and **2** are ascribed at around 71.61 ppm and 72.55 ppm respectively. The signals arousing at 125.38 ppm and 133.09 ppm are attributed to the unsaturated (sp^2) carbons of fatty acid chain of **1**. The peak at 175.63 ppm is accredited to the amide carbonyl carbon of **1** [20, 22, 23].

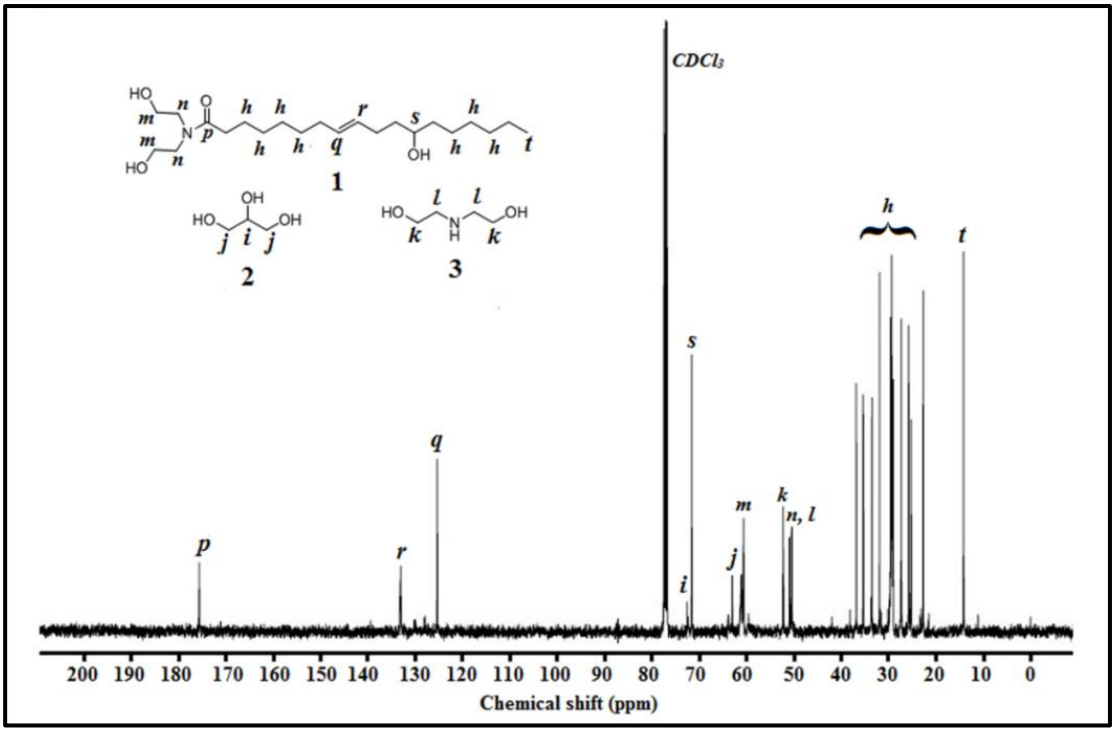

Figure 2.3. ^{13}C NMR spectrum of COMP.

2.3.3. Synthesis of HPU

HPU was synthesized by a two-step, one-pot polymerization reaction using COMP as the multi-functional branching moiety, following the A_x+B_y (x, y ≥2) approach. **Scheme 2.2** illustrates the synthesis of HPU. In the first step, macroglycol PCL was reacted with diisocyanate IPDI to form a -NCO terminated pre-polymer by maintaining NCO/OH ratio of 1.5. In this step, the macroglycol undergoes nucleophillic addition to the diisocyanate to generate linear urethane linkages. The first step was carried out in 15% dilution (xylene as solvent) only as the reactants were di-functional entities. The –NCO terminated pre-polymer then was reacted simultaneously with both the multi-branching unit COMP and chain extender MGE in the second step to yield HPU. In this step, the –NCO terminated pre-polymer undergoes further linear chain extension of urethane linkages with MGE and highly branching chain extension with COMP. This step is very crucial because it leads to the development of the dendritic, linear and terminal units of HPU. The NCO/OH ratio of 1 was maintained throughout the second step. The addition of the multi-branching unit was

carefully handled in order to avoid gel formation. This was done by sustaining the reaction in 40% dilution (xylene as solvent). The reaction was preserved beautifully even at an elevated temperature without signs of gel formation, owing to the presence of aliphatic moieties. The completion of the reaction was indicated by the absence of free –NCO band at 2270 cm^{-1} in the FT-IR spectrum of the reaction mixture taken directly without any purification. Different compositions of HPU were prepared in similar fashion by varying the content of multi-functional moiety COMP. Notably, the time required for the synthesis of HPUs was more compared to the linear analogs, due to the presence of low reactive aliphatic groups in renewable resource based precursors. Polymerization reactions in PU mostly correspond to step-growth polymerization. Unlike that of addition polymerization, there is no elimination of small molecules. Hence, it is also often referred as rearrangement polymerization [9].

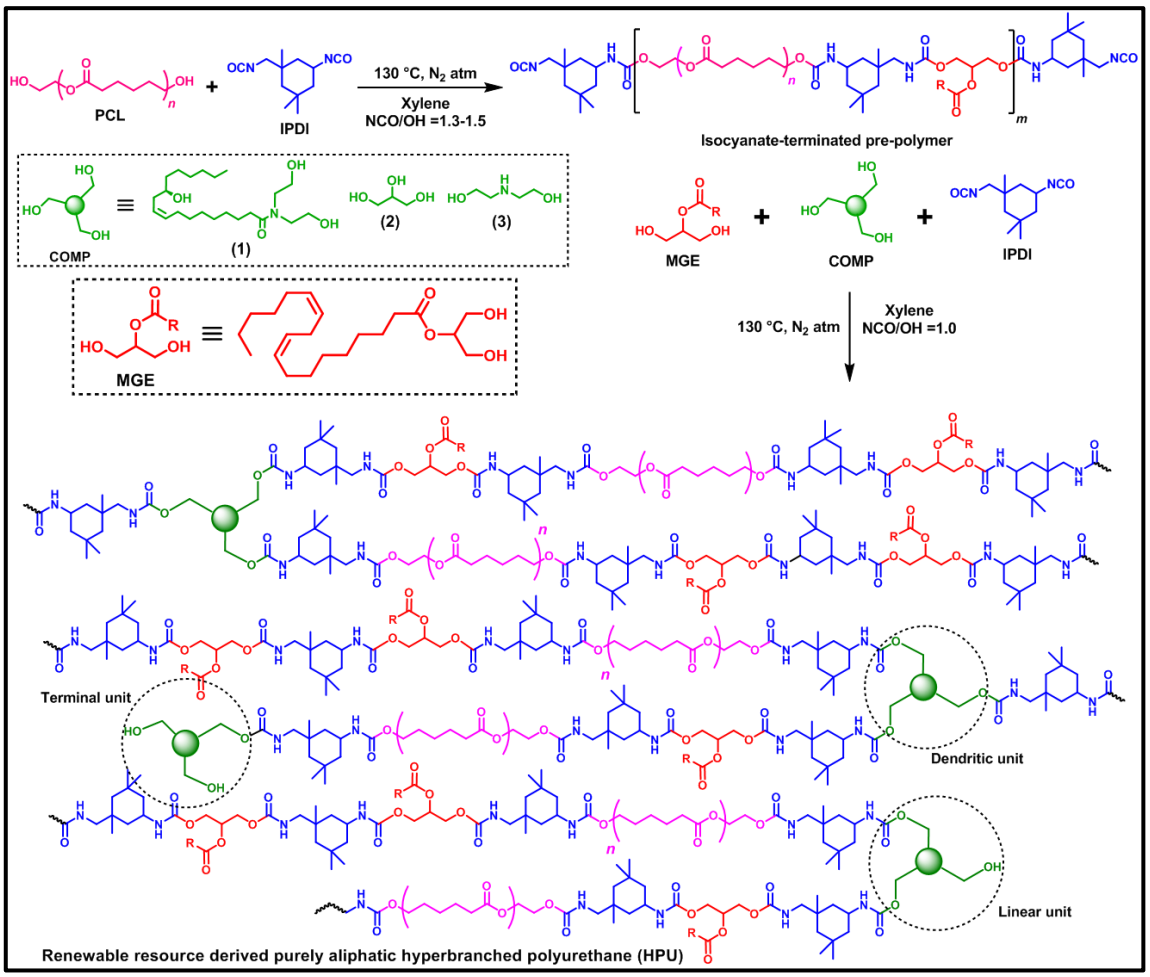

Scheme 2.2. Synthesis of HPU.

2.3.4. Characterization of HPU

2.3.4.1. FT-IR study

FT-IR spectroscopy was employed to detect the chemical linkages in the structures of the synthesized PUs. FT-IR spectrum of the initially synthesized pre-polymer in **Figure 2.4.a** displayed the presence of a sharp free –NCO band at 2270 cm^{-1}, consistent with the formation of an isocyanate-terminated pre-polymer [12]. The FT-IR spectra of synthesized PUs, presented in **Figure 2.4.b** displayed the presence of characteristic bands associated with PU [6, 7, 12]. The absence of the band for free –NCO at 2270-2250 cm^{-1} indicates the completion of the reaction, as mentioned previously. The band appearing at 3441-3450 cm^{-1} is due to overlapping –NH and –OH stretching vibrations. A small band appears at 1735 cm^{-1} for the ester –C=O stretching and the sharp band emerges at 1637 cm^{-1} is due to amide –C=O stretching vibrations. While the band appears at 1031 cm^{-1} for –O–C=O stretching vibrations. All of these bands indicate the existence of the characteristic urethane linkage in the macromolecule. The two bands appearing at 2920-2932 cm^{-1} and 2851-2857 cm^{-1} are assigned for symmetric and asymmetric vibrations of $–CH_2$, respectively. The prominently featuring medium band near 1471 cm^{-1} is an outcome of C-H bending vibrations. Thus, the study confirms the presence of urethane linkages along with other significant linkages [6, 7].

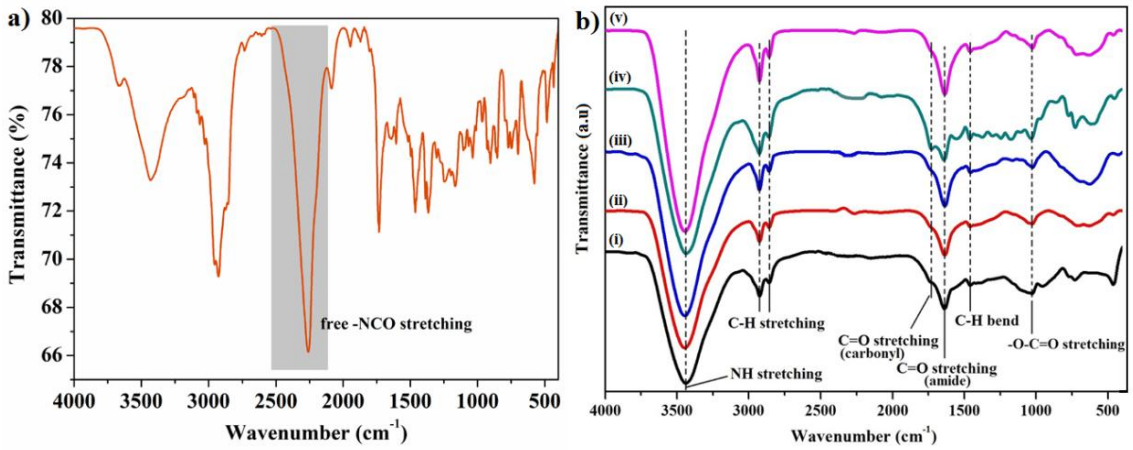

Figure 2.4. a) FT-IR spectrum of isocyanate-terminated pre-polymer, and **b)** FT-IR spectra of (i) HPU1, (ii) HPU2, (iii) HPU3, (iv) BLPU and (v) LPU.

2.3.4.2. NMR study

It is difficult to fully interpret the ^1H NMR spectrum of HPU, due to the existence of IPDI in two isomeric forms (*E* and *Z*), along with two different kinds of isocyanate groups (primary –NCO and secondary –NCO). As a result, IPDI displays variable selectivity towards urethane reaction under different conditions [24]. Nonetheless, the ^1H NMR data provide compelling evidence towards the presence of urethane linkage, fatty acid chain of MGE, COMP and PCL moieties. This suggested the formation of the proposed hyperbranched HPU

structure. The ^{1}H NMR spectrum of HPU is presented in **Figure 2.5**.

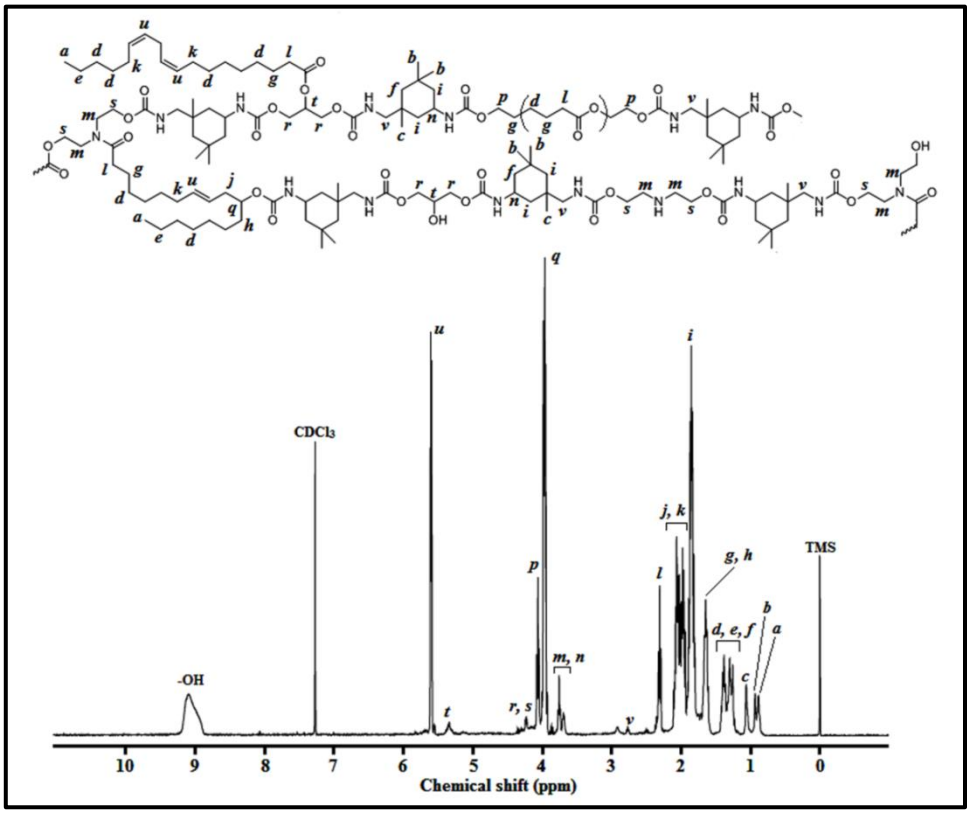

Figure 2.5. ^{1}H NMR spectrum of HPU.

The signals originating at 0.89 ppm, 0.93 ppm and 1.06 ppm are due to the terminal methyl (-CH_3) groups of the fatty acid moieties of MGE and COMP, and methyl groups of IPDI, respectively [7, 20, 25]. The peaks appearing at 1.26 ppm and 1.30 ppm belong to the internal methylene (-CH_2) groups of fatty acid chains of MGE, COMP, PCL moieties. The methylene protons of IPDI emerge at 1.40 ppm and 1.85 ppm [25]. The peaks at 1.98 ppm, 2.06 ppm and 2.31 ppm are attributed to the allylic (=C-CH) protons and alpha methylene protons (α –CH_2) to C=O of the fatty acid chains of COMP and MGE, respectively [7, 20]. The methylene (-CH_2) protons adjacent to the urethane linkage appear at 2.91 ppm. The methylene protons and methine (-CH) protons attached with amide group of COMP and urethane linkage correspond to peaks at 3.70 ppm and 3.76 ppm [6, 7]. The multiple peaks appearing at 3.96 ppm, 4.06 ppm and 4.22 ppm belong to the methine proton adjacent to –OH bond of COMP and methylene protons (O-CH_2) attached to urethane linkages formed by PCL, MGE and COMP respectively. The protons attached to C=C of the fatty acid moieties of COMP and MGE appear at 5.61 ppm. The free hydroxyl groups of polymeric chain appear as a broad peak at 9.13 ppm [26]. However, the quantitative assessment of the ^{1}H NMR spectrum of HPU doesn't provide information about the degree of branching as the peaks of

interest appear as complex aggregates. However, use of a branching template make the whole process highly viable towards the formation of hyperbranched architecture.

2.3.4.3. XRD study

XRD analysis confirmed the presence of crystallinity in the PUs, as illustrated by sharp diffraction patterns in **Figure 2.6**. The analysis revealed the presence of two strong diffractions at 2θ = 21.2° and 2θ = 23.5° corresponding to the lattice planes (1 1 0) and (2 0 0) of crystalline moiety of PCL in the macromolecule [6]. All the PUs exhibited the same diffraction patterns, because of presence of PCL. However there is a minute shift in the diffraction peaks of HPUs and BLPU compared to only LPU, which can be attributed to the presence of renewable resource based components, in addition to PCL. In addition, reduction in diffraction pattern intensity of HPUs is observed with the increase in percentage content of COMP. This can be attributed to the hyperbranched architecture of HPUs resulting in comparatively less efficient packing of crystalline PCL moiety, in contrast to regularly structured LPUs [6, 7].

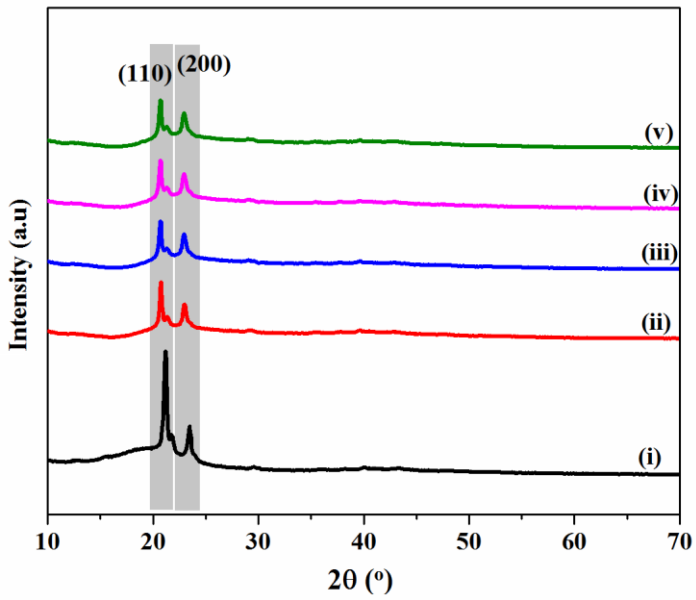

Figure 2.6. XRD patterns of (i) LPU, (ii) BLPU, (iii) HPU1, (iv) HPU2 and (v) HPU3.

2.3.5. Physical properties

The physical properties of HPU were investigated to gauge a better understanding of the structure of the polymer. HPU was soluble in polar aprotic solvents like THF, DMF, DMAc, DMSO, acetone, etc. as well as in halogenated solvents like chloroform, DCM, etc. This can be accredited to the globular structure of HPUs and the presence of polar surface and terminal groups on the polymer backbone, offering better dissolution in different solvents

[27]. However, HPU was insoluble in protic solvents such as water and alcohols. Molecular weights of HPU were found to be high, as in order of 10^4. Number average (M_n) and weight average (M_w) molecular weight of HPU1 were found to be around 2.59 x 10^4 g mol^{-1} and 3.75 x 10^4 g mol^{-1} respectively, with polydispersity index (PDI) of 1.44. However, the actual molecular weight may be more than the cited value as linear polystyrene standard was used. Attainment of such high molecular weight pointed towards the formation of a hyperbranched structure, with three-dimensional irregular chain segments. The specific gravity of HPU was found to in the range of 1.01-1.06, owing to its high molecular weight and compact hyperbranched structure. Additionally, the specific gravity of HPU showed increasing values with increase in percentage of COMP. This slight variation can be justified by the increase in the ratio of hard segment, thereby raising the density through various polar interactions in the polymer chains, leading to the compactness of the structure [6, 11]. The color of HPU was yellow, which was mainly due to the color of the renewable vegetable oil-based precursors. HPU films mostly displayed modest transparency, due to the presence of purely aliphatic precursors.

2.3.6. Mechanical properties

The mechanical properties of the synthesized PUs are illustrated in **Table 2.2.** The mechanical performance of PU depends on various factors such as presence of polar linkages like urethane, ester, etc. in the polymer matrix, degree of urethane linkages, physical/chemical cross-linking, physical state of the polymer during testing, molecular weight and its distribution, and various physico-chemical interactions involved in the polymer matrix such as hydrogen bonding, polar-polar interactions, etc [11-13].

Table 2.2. Mechanical properties of PUs

Composition	**LPU**	**BLPU**	**HPU1**	**HPU2**	**HPU3**
Tensile strength (MPa)	3.6±0.4	4.1±0.1	4.3±0.2	4.6±0.1	5.3±0.1
Elongation at break (%)	361±20	625±10	668±20	625±5	632±10
Toughness[a] (MJ m^{-3})	12.00±0.5	26.18±0.2	27.06±0.5	27.97±0.1	32.16±0.2
Scratch hardness[b] (kg)	4.5±0.5	5.0±0.5	6.0±0.5	7.2±0.5	10.0±0.5
Impact resistance[c] (kJ m^{-1})	13.68	15.06	16.56	18.45	19.02

[a]calculated by integrating the stress-strain profiles. [b]maximum limit of the instrument is 10 kg. [c]calculated by converting to energy units per thickness of PU films.

HPUs demonstrated superior mechanical properties than their linear counterparts. HPUs demonstrated enhanced tensile strength in comparison to LPUs, and followed an increasing trend with the increase in percentage content of COMP. This enhancement can be attributed to the unique three-dimensional structure of HPUs having large number of polar functional moieties in the polymeric chains. These numerous polar functional moieties resulted in stronger physico-chemical interaction within the polymer network, imparting rigidity to the HPU structure [11]. At the same time, HPUs displayed very high elongation at break in comparison to LPUs, although the values showed a receding pattern with the increase in content of COMP. This view is endorsed by the flexibility of the polymeric chains due to the presence of long chain aliphatic moieties; however the inherent rigidity of the structure caused through a variety of secondary interactions in the polymer chains affects the flexibility [6]. The corresponding stress-strain profile reflects the aforementioned observations of the HPUs, as seen in **Figure 2.7**. Integration of the stress-strain profiles of PUs revealed high values of toughness of HPUs, compared to the linear ones. Since, toughness is the combination of a material's rigidity and flexibility, therefore enhanced tensile strength and very high elongation at break of HPUs can be credited for the same [6, 11]. HPUs exhibited high scratch hardness than LPUs, courtesy of their superior toughness. In the same vein, the impact resistance of HPUs was found to be dominant over the linear analogs, which can be attributed to high angle of toughness of the HPUs, i.e. the ability to absorb the applied external energy and reimburse it to its molecular network [6]. The formation of hyperbranched architecture assists in the absorption and distribution of the impact energy, thereby increasing the durability of HPUs.

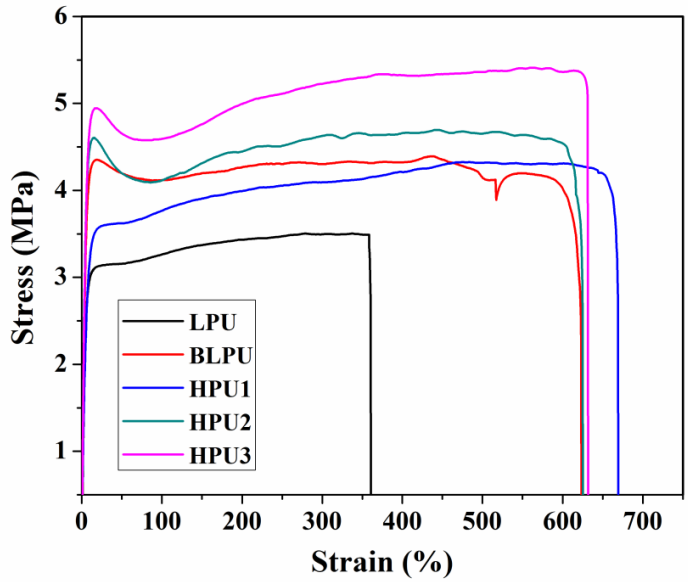

Figure 2.7. Stress-strain profiles of PUs**.**

2.3.7. Thermal properties

The thermal properties of the synthesized PUs were assessed using TGA and DSC. The thermal stability of PU is influenced by the composition of the hard and soft segments, degree of the urethane linkage, extent of physical/chemical crosslinking, crystallinity and molecular weight and its distribution [6, 7]. TG and their first derivative curves illustrated in **Figure 2.8.a** and **2.8.b** revealed that HPUs and BLPU undergo a two-step degradation pattern, while synthetic LPU undergo single step degradation. The first step degradation of HPUs is attributed to the bio-based aliphatic fatty acid chains of the monoglyceride and COMP in the structure [28, 29]. The second step degradation is ascribed to the urethane linkage and ester groups of HPUs [6, 28]. In case of synthetic LPU, the single step degradation is attributed to the thermal decomposition of urethane linkages.

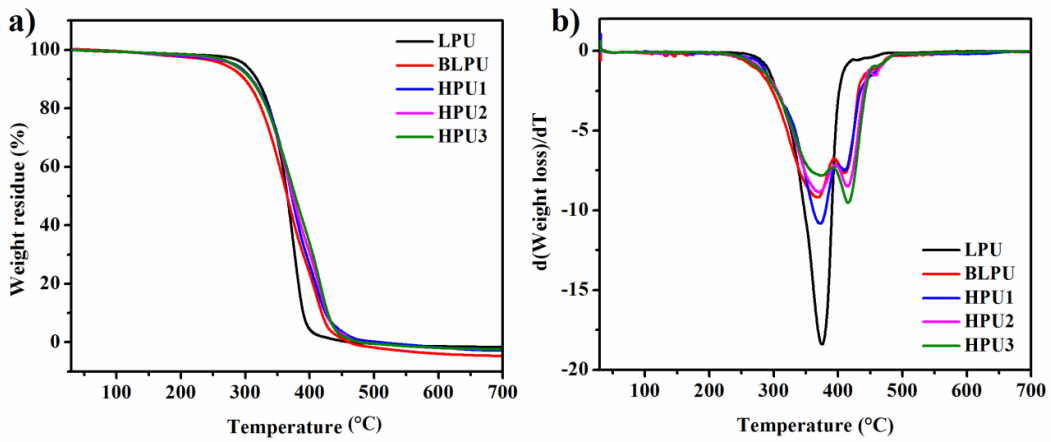

Figure 2.8. a) TG curves, and **b)** dTG curves of PUs.

The onset (T_{onset}), maximum (T_{max}) and endset (T_{endset}) degradation temperatures of the PUs are shown in **Table 2.3.** HPUs demonstrated higher thermal degradation temperatures than their linear analogs, indicating their higher thermal stability. Moreover, the degradation temperatures of HPUs showed increase with increase in content of COMP. The good thermal stability of HPU can be attributed to hyperbranched architecture, hindering the decomposition of the polymer matrix by crosslinking and secondary interactions [6, 7].

Table 2.3. Thermal degradation temperatures of PUs

Parameter	LPU	BLPU	HPU1	HPU2	HPU3
T_{onset} (°C)	279	275	280	283	285
T_{max} (1st step) (°C)	374	368	372	372	372
T_{max} (2nd step) (°C)	-	409	410	414	416
T_{endset} (°C)	409	435	442	448	453

DSC curves illustrated in **Figure 2.9**, showed that HPU possess dual glass transition temperature and melting temperature. The dual glass transition temperature of HPUs can be attributed to the existence of hard and soft segments in their structure [28, 29]. These segments are constituted of purely aliphatic units and contribute to the overall structural integrity of HPUs. The glass transition temperatures (T_g and $T_{g'}$) and melting temperature (T_m) of HPUs are reported in **Table 2.4.** The first glass transition temperature at around -50 °C can be ascribed to the PCL moiety in the soft segments of HPU, while the second glass transition temperature around 0 °C may be due to renewable source based aliphatic moieties present in the hard segments of HPU. Surprisingly, it was seen that both T_g and $T_{g'}$ of the HPUs were found to be at very low temperature. This anomaly may have arisen due to the plasticization effect of the aliphatic moieties present in the polymer chains [30, 31]. In similar vein, the melting temperature of HPU can be attributed to the crystalline PCL moiety that has a melting point close to 50 °C. DSC curves further revealed that T_m of the HPUs followed a decreasing pattern with respect to the content of COMP, with the intensity of the T_m vary directly with wt% of COMP. The compactness of HPU structure may have influence the values of T_m to vary in this fashion.

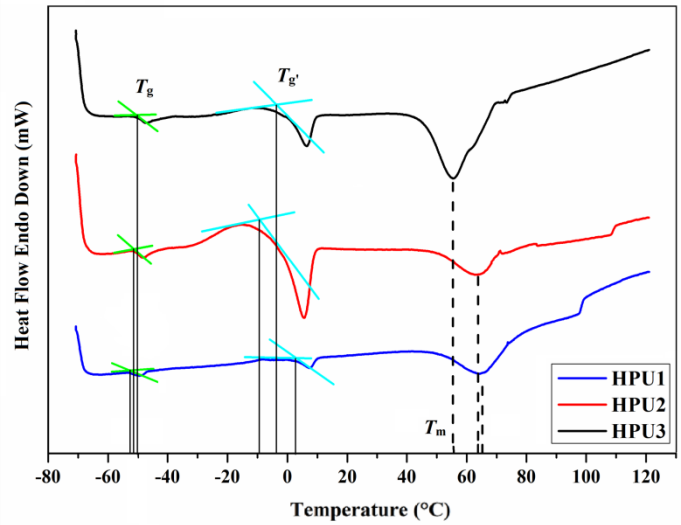

Figure 2.9. DSC curves of HPUs.

Table 2.4. Glass transition and melting temperature of HPUs

Parameter	LPU	BLPU	HPU1	HPU2	HPU3
T_g (1st) (°C)	-51.7	-50.9	-50.6	-50.3	-50.4
$T_{g'}$ (2nd) (°C)	6.5	0.9	2.99	-2.8	-0.7
T_m (°C)	48.3	57.4	64.2	63.4	55.5

2.3.8. Chemical resistance study

The chemical resistance of PUs was tested in different chemical environments *viz*. 10% aqueous NaCl (w/v), 20% aqueous ethanol (v/v), 5% aqueous HCl (v/v), 3% NaOH (w/v) and normal tap water. The results of these chemical resistance tests are reported in **Table 2.5**. HPUs exhibited superior chemical resistance in all the tested chemical environments, in comparison to their linear analogs. Interestingly, HPUs show better chemical resistance to alkali, even though it possesses hydrolysable ester linkages in the monoglyceride and PCL moieties of the macromolecule. This good chemical resistance of HPUs can be mainly attributed to the hyperbranched architecture leading to greater extent of physical/chemical crosslinking and various secondary interactions like hydrogen bonding, polar-polar interactions, etc. in the PU matrix [6, 12].

Table 2.5. Weight loss (%) of PUs in different chemical media

Polymer	10% NaCl	20% EtOH	5% HCl	3% NaOH	Tap Water
HPU1	0.020	0.033	0.042	0.481	0.0
HPU2	0.018	0.028	0.040	0.434	0.0
HPU3	0.013	0.011	0.039	0.375	0.0
BLPU	0.022	0.031	0.049	4.325	0.0
LPU	0.029	0.033	0.055	5.050	0.0

2.3.9. Biodegradation study

Biodegradation of the PUs was studied by exposing the PU films to a bacterial strain of *P. aerugonisa* in a nutrient medium. OD measurement of the bacterial culture media upto 7 consecutive weeks, as shown in **Figure 2.10.a** indicated higher biodegradability of HPU than that of linear analogs. Further, HPUs undergo substantial biodegradation than LPUs, as notably reflected in the percent weight loss of the HPUs recorded after 7 weeks of exposure to the bacterial strain in **Figure 2.10.b**. The overall biodegradability of HPU can be attributed to the hyperbranched structure of the macromolecule and presence of renewable resource precursors with more hydrolysable linkages in the polymer backbone. The well expanded hyperbranched architecture and presence of larger number of hydrolysable ester linkage in HPUs provides a better liable surface for bacterial adhesion and growth [7, 19]. Additionally, the biodegradability of HPU showed improvement with increase in percentage of renewable resource precursor COMP. The biodegradation was

found to be the highest for HPU3 as it contains the highest content of COMP, while LPU with no renewable component and lesser hydrolysable ester linkage exhibited the lowest biodegradation. SEM micrographs of HPU in **Figure 2.10.c** and **Figure 2.10.d** further justified this observation showing significant bacterial adherence and surface erosion, compared to the control.

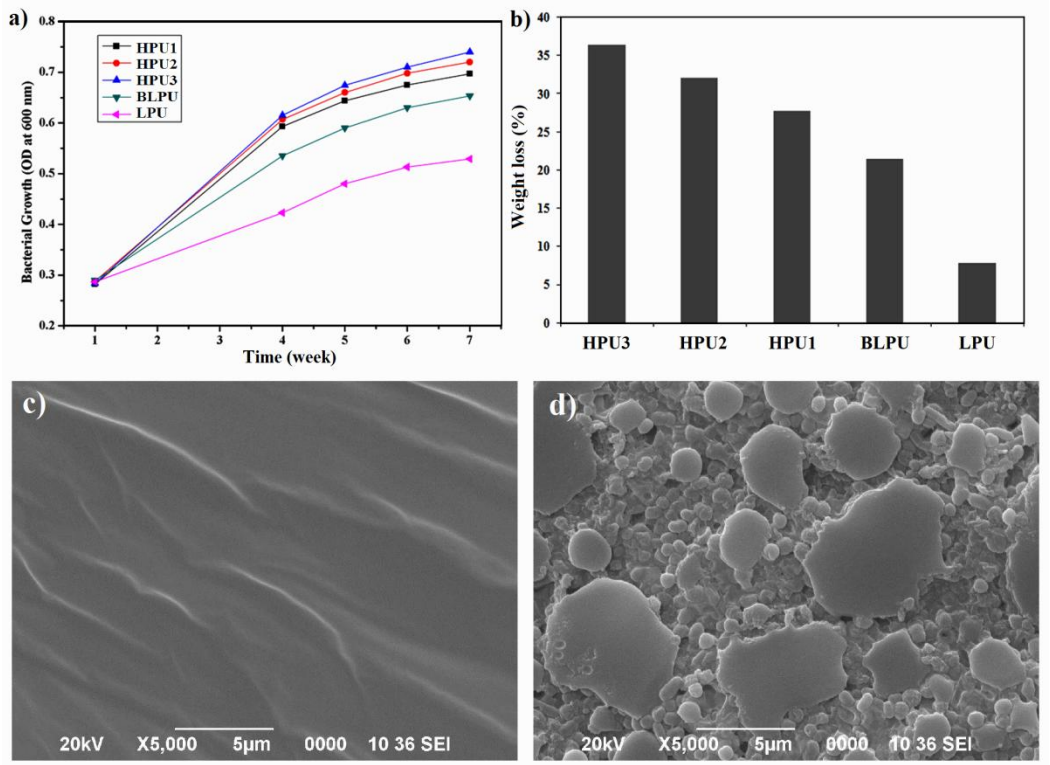

Figure 2.10. a) Optical density (OD) plots showing growth of *P. aerugonisa* bacterial strain against time for PUs during initial 7 weeks, **b)** Weight losses of PU films after 7 weeks of exposure to *P. aerugonisa* strain and SEM micrographs of HPU film **c)** before and **d)** after biodegradation.

2.3.10. UV-resistance study

UV-aging of PUs was conducted by exposing their films to UV light of wavelength 254 nm for a period of 2 weeks. Evaluation of mechanical properties of PU films before and after UV-aging displayed slight variations in case of HPUs compared to that of LPUs. In comparison to LPUs, HPUs exhibited almost comparable values of tensile strength, while there are some variations in elongation at break and toughness, as seen in the corresponding histograms in **Figure 2.11**. This variation may be attributed to enhancement of crosslinking and degradation of the polymer matrix simultaneously caused by UV irradiation [32]. However, this variation was less prolific in HPUs than LPUs, indicating their better resistance to UV-aging. This better resistance to UV-aging displayed by HPU

was further reflected in the percentage retention of their mechanical properties, as shown in **Table 2.6**. HPUs demonstrated very high percentage retention of tensile strength (~98%), elongation at break (~88%) and toughness (87%). Especially, the percentage retention of elongation at break and toughness was considerably superior to LPUs. This superior percentage retention of mechanical properties reflected better UV-resistance of HPUs. This superiority can be attributed to the hyperbranched architecture of HPU imparting more mechanical stability than the linear counterparts. This mechanical stability is further complimented by the purely aliphatic nature of HPU matrix containing lesser UV-light absorbing groups, thereby providing more stability to UV degradation [32].

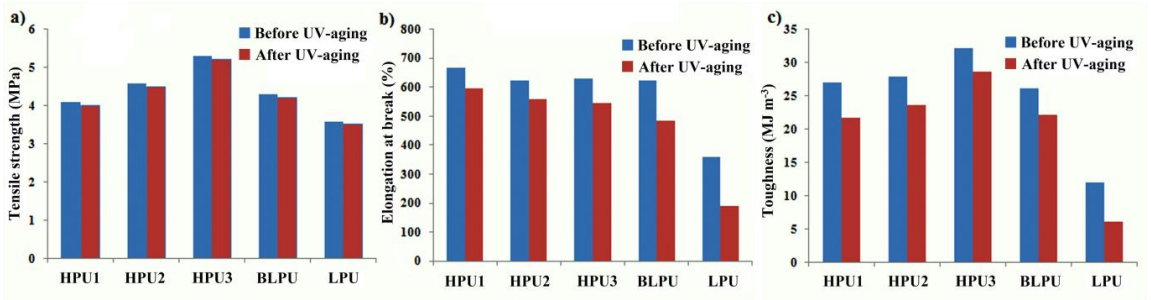

Figure 2.11. Histograms showing **a)** tensile strength, **b)** elongation at break, and **c)** toughness of PUs before, and after UV-aging.

Table 2.6. Retention (%) of mechanical properties of PUs after UV-aging

Parameter	LPU	BLPU	HPU1	HPU2	HPU3
Tensile strength	97.14	97.67	97.50	97.70	98.07
Elongation at break	10.99	71.13	88.10	88.59	84.03
Toughness	4.87	82.33	75.29	81.83	87.63

2.3.11. Shape memory study

Shape memory behavior of PU was examined by temporarily altering the shape of the PU films and then recovering the original shape by application of different external stimuli. This shape memory attribute of PU is a manifestation of entropy of the macromolecule [33, 34]. The PU films in their original shapes have their molecular chains arranged in an arbitrary chain conformation i.e. a high entropy state. Upon heating the films at 65 °C (>T_m), the mobility of these chains become dynamic, as a result of which the entropy rises and the films can be deformed into a temporary ring shape. Subsequently, the temporary shape is fixed by freezing the sample in an ice water-salt bath at -5 °C (<$T_{g'}$) for 15 mins. In this state, the polymer films lose its dynamicity caused by the freezing of the molecular chains of the

macromolecule in the temporary deformed state and entropy lowers. Now, on application of different external stimuli *viz.* thermal energy, microwave and sunlight, the dynamicity of the molecular chains increases, leading to gain in entropy and thereby regaining of the original shape [13, 35].

HPUs demonstrated multi-stimuli responsive shape memory behavior under thermal heating, microwave and sunlight. The shape fixity, shape recovery and shape recovery time under thermal heating, microwave and sunlight are presented in **Table 2.7**. HPUs exhibited excellent shape fixity compared to LPUs, owing to their hyperbranched structure with enhanced physico-chemical crosslinking and secondary interactions among the polymer segments in the temporary fixed orientation. HPUs displayed better shape recovery and lesser shape recovery time, in comparison to LPU. Further, the shape recovery time of HPU increased with percentage content of COMP. The better shape recovery of HPU can be attributed to the increased amount of stored energy in the system, due to its hyperbranched structure with uniform distribution of hard-soft segments and enhanced secondary interactions [13]. The hyperbranched structure allowed faster dissipation of stored energy throughout its molecular network, contributing to the shape recovery process [13, 35]. Moreover, the shape recovery of HPU was found to be expeditious in case of thermal heating and microwave as the stimuli, in comparison to sunlight. Shape memory behavior of HPU2 under thermal heating is illustrated in **Figure 2.12**.

Table 2.7. Shape memory behavior of PUs

Stimulus	Shape memory parameter	**HPU1**	**HPU2**	**HPU3**	**BLPU**	**LPU**
Thermal	Shape fixity (%)	95.7	96.1	96.3	87.8	72.4
	Shape recovery time (s)	21	20	20	25	42
	Shape recovery (%)	96.8	96.9	97.1	95.5	90.5
Microwave	Shape fixity (%)	95.5	96.1	96.7	85.1	70.8
	Shape recovery time (s)	95	91	91	130	156
	Shape recovery (%)	96.5	96.3	98.2	95.1	90
Sunlight	Shape fixity (%)	95.1	95.7	94.3	88.0	70.7
	Shape recovery time (min)	21	19.2	15.7	27	30
	Shape recovery (%)	96.1	96.7	96.4	88.2	72.5

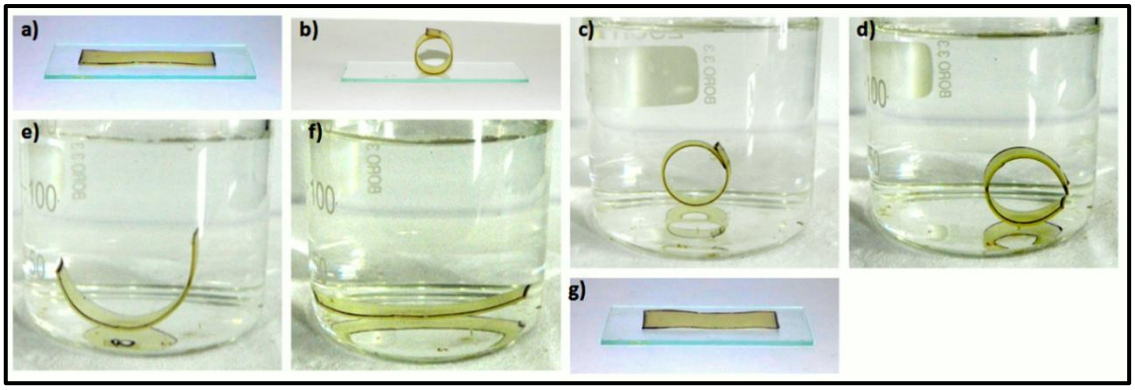

Figure 2.12. Digital images displaying the shape memory behavior of HPU2: **a)** Original shape, **b)** temporary fixed shape at room temperature, **c)–f)** shapes at 50 °C in 5s, 10s, 15s, 20s and **g)** regained original shape at room temperature.

2.4. Conclusion

The current chapter describes the utility of castor oil-modified polyol as a renewable precursor for the synthesis of HPU. Purely aliphatic HPU is successfully synthesized by following pre-polymerization technique, following the A_x+B_y (x, y ≥2) approach. The composition of the castor oil-modified polyol is varied and optimized in the study. Various spectroscopic, microscopic and analytical techniques help in establishing the structural composition of the HPU. The synthesized HPUs demonstrated superior mechanical properties, thermal properties and chemical resistance than their linear analogs. Remarkably, HPU displayed profound biodegradability, significant resistance to UV-aging and excellent multi-stimuli responsive shape memory behavior. The unique hyperbranched architecture and purely aliphatic nature of the polymer matrix imparted considerable advantage to the HPU. Thus, the synthesized polymer possesses remarkable potential as a multi-faceted material for advanced applications. Further, from the overall results, the performance of HPU with highest content of castor oil-modified polyol, i.e. HPU3 was found to be optimum and henceforth it is used as the matrix for the fabrication of different nanocomposites in the subsequent chapters with the general coding of HPU.

References

[1] Zhu, Y., Romain, C., and Williams, C. K. Sustainable polymers from renewable resources. *Nature*, 540(7633):354, 2016.

[2] Gandini, A. Polymers from renewable resources: a challenge for the future of macromolecular materials. *Macromolecules*, 41(24):9491-9504, 2008.

[3] Xia, Y. and Larock, R. C. Vegetable oil-based polymeric materials: synthesis, properties and applications. *Green Chemistry*, 12(11):1893-1909, 2010.

[4] Pfister D. P., Xia Y., Larock R. C. Recent advances in vegetable oil-based polyurethanes. *ChemSusChem*, 4(6):703-17, 2011.

[5] Lu, Y. and Larock, R. C. Soybean-oil-based waterborne polyurethane dispersions: effects of polyol functionality and hard segment content on properties. *Biomacromolecules*, 9(11):3332-3340, 2008.

[6] Thakur, S. and Karak, N. Castor oil-based hyperbranched polyurethanes as advanced surface coating materials. *Progress in Organic Coatings*, 76(1):157-164, 2013.

[7] Das, B., Konwar, U., Mandal, M., and Karak, N. Sunflower oil based biodegradable hyperbranched polyurethane as a thin film material. *Industrial Crops and Products*, 44:396-404, 2013.

[8] Kumar, A. and Ramakrishnan, S. Hyperbranched polyurethanes with varying spacer segments between the branching points. *Journal of Polymer Science A: Polymer Chemistry*, 34(5):839-848, 1996.

[9] Spindler, R. and Frechet, J. M. Synthesis and characterization of hyperbranched polyurethanes prepared from blocked isocyanate monomers by step-growth polymerization. *Macromolecules*, 26(18):4809-4813, 1993.

[10] Hong, L., Cui, Y., Wang, X., and Tang, X. Synthesis of a novel one-pot approach of hyperbranched polyurethanes and their properties. *Journal of Polymer Science Part A: Polymer Chemistry*, 40(3):344-350, 2002.

[11] Deka, H. and Karak, N. Bio-based hyperbranched polyurethanes for surface coating applications. *Progress in Organic Coatings*, 66(3):192-198, 2009.

[12] Karak, N., Rana, S., and Cho, J. W. Synthesis and characterization of castor-oil-modified hyperbranched polyurethanes. *Journal of Applied Polymer Science*, 112(2):736-743, 2009.

[13] Kalita, H. and Karak, N. Bio-based elastomeric hyperbranched polyurethanes for shape memory application. *Iranian Polymer Journal*, 21(4):263-271, 2012.

[14] Voit, B. I. and Lederer, A. Hyperbranched and highly branched polymer architectures synthetic strategies and major characterization aspects. *Chemical Reviews*, 109(11):5924-5973, 2009.

[15] Gao, C. and Yan, D. A_2+CB_n Approach to hyperbranched polymers with alternating ureido and urethano units. *Macromolecules*, 3(3):613-620, 2003.

[16] Singh, R. P., Tomer, N. S., and Bhadraiah, S. V. Photo-oxidation studies on polyurethane coating: effect of additives on yellowing of polyurethane. *Polymer Degradation and Stability*, 73(3):443-446, 2001.

[17] Irusta, L. and Fernandez-Berridi, M. J. Photooxidative behaviour of segmented aliphatic polyurethane. *Polymer Degradation and Stability*, 63(1):113-119, 1991.

[18] Dutta, S. and Karak, N. Effect of the NCO/OH ratio on the properties of *Mesua ferrea* L. seed oil-modified polyurethane resins. *Polymer International*, 55(1):49-56, 2006.

[19] Das, B., Chattopadhyay, P., Mandal, M., Voit, B., and Karak, N. Bio-based biodegradable and biocompatible hyperbranched polyurethane: a scaffold for tissue engineering. *Macromolecular Bioscience*, 13(1):126-139, 2013.

[20] Pramanik, S., Sagar, K., Konwar, B. K., and Karak, N. Synthesis, characterization and properties of a castor oil modified biodegradable poly(ester amide) resin. *Progress in Organic Coatings,* 75(4):569-578, 2012.

[21] Ahmad, S., Ashraf, S. M., and Zafar, F. Development of linseed oil based polyesteramide without organic solvent at lower temperature. *Journal of Applied Polymer Science*, 104(2):1143-1148, 2007.

[22] Malavolti, M., Brandi, A., Salvini, A., and Giomi, D. Transesterification of castor oil with trimethylchlorosilane: simultaneous formation of fatty acid alkyl esters and α-monochlorohydrin. *RSC Advances*, 5(94):77341-77347, 2015.

[23] Böttinger, W., Maiwald, M., and Hasse, H. Online NMR spectroscopic study of species distribution in MEA–H_2O–CO_2 and DEA–H2O–CO_2. *Fluid Phase Equilibria*, 263(2):131-143, 2008.

[24] Lomölder, R., Plogmann, F., and Speier, P. Selectivity of isophorone diisocyanate in the urethane reaction influence of temperature, catalysis, and reaction partners. *Journal of Coatings Technology*, 69(868):51-57, 1997.

[25] Gogoi, S., Barua, S., and Karak, N. Biodegradable and thermostable synthetic hyperbranched poly(urethane-urea)s as advanced surface coating materials. *Progress in Organic Coatings*, 77(9):1418-1427, 2014.

[26] Gogoi, S. and Karak, N. Biobased biodegradable waterborne hyperbranched polyurethane as an ecofriendly sustainable material. *ACS Sustainable Chemistry & Engineering*, 2(12):2730-2738, 2014.

[27] Yates, C. Y. and Hayes, W. Synthesis and applications of hyperbranched polymers. *European Polymer Journal*, 40(7):1257-1281, 2004.

[28] Javni, I., Petrović, Z. S., Guo, A., and Fuller, R. Thermal stability of polyurethanes based on vegetable oils. *Journal of Applied Polymer Science*, 77(8):1723-1734, 2000.

[29] Ristić, I. S., Bjelović, Z. D., Holló, B., Szécsényi, K. M., Budinski-Simendić, J., Lazić, N., and Kićanović, M. Thermal stability of polyurethane materials based on castor oil as polyol component. *Journal of Thermal Analysis and Calorimetry*, 111(2):1083-1091, 2013.

[30] Immergut, E. H. and Mark, H. F. Principles of Plasticization. *Advances in Chemistry,* 48:1-26, 1965.

[31] Zlatanić, A., Lava, C., Zhang, W., and Petrović, Z. S. Effect of structure on properties of polyols and polyurethanes based on different vegetable oils. *Journal of Polymer Science Part B: Polymer Physics*, 42(5):809-819, 2004.

[32] Das, S., Pandey, P., Mohanty, S., and Nayak, S. K. Study of UV aging on the performance characteristics of vegetable oil and palm oil derived isocyanate based polyurethane. *Korean Journal of Chemical Engineering*, 34(2):523-538, 2017.

[33] Kim, B. K., Lee, S. Y., and Xu, M. Polyurethanes having shape memory effects. *Polymer*, 37(26):5781-5793, 1996.

[34] Xie, T. Recent advances in polymer shape memory. *Polymer*, 52(22):4985-5000, 2011.

[35] Kalita, H. and Karak, N. Biobased hyperbranched shape-memory polyurethanes: effect of different vegetable oils. *Journal of Applied Polymer Science*, 131(1):39579, 2014.